Composites Science and Technology xxx (xxxx) 110515

Contents lists available at ScienceDirect

Composites Science and Technology

journal homepage: www.elsevier.com/locate/compscitech

Impact behaviour of bio-inspired sandwich panels integrally manufactured from 3D printed continuous carbon fibre reinforced polyamide

I. Sukia [a,*], A. Esnaola [a], B. Erice [a,b], J. Aurrekoetxea [a]

[a] Mechanical and Industrial Production Department, Mondragon University, Loramendi 4, 20500, Mondragón, Spain
[b] IKERBASQUE, Basque Foundation for Science, Bilbao, Spain

ARTICLE INFO

Keywords:
Impact behaviour (B)
3D printed composites (A)
Bioinspired sandwich
Functional graded structure
Sandwich structures (C)

ABSTRACT

This paper studies the effect of several design parameters on the impact performance of fully 3D printed sandwich panels with a core cell unit inspired by the trabecular structure of the forewing of a beetle. The key finding is that the asymmetric sandwich panel, which featured a thicker face sheet at the back and a core with a variating cell wall thickness of weak-to-strong, exhibited the highest impact energy dissipation. Specifically, 98.1 J was dissipated with 6970 N of peak load. This surpassed the performance of the sandwich panel with homogeneous cell wall thickness and asymmetric face sheets, which dissipated only 72.1 J and failed at 5406 N. In general, asymmetric configurations were found to dissipate greater energy than symmetric face sheets, and for sandwich plates with homogenous cores, the configuration with the thickest back face sheet proved more resistant to damage than the opposite asymmetric configuration.

1. Introduction

Sandwich panels are considered lightweight materials in several sectors such as aeronautics [1], railway, marine, and automotive [2]. Their high stiffness-to-weight and strength-to-weight ratios, impact energy absorption capacity, and thermal insulation can be tailored to the requirements of each product. Design variables include a range of face sheet materials (composites, lightweight alloys) and cellular cores [3], multiple relative face-to-core thicknesses, and architectures with symmetric or asymmetric face sheets combinations of which deliver multiple optimisation solutions for the structural engineer [3]. Recent studies suggest that the energy absorption capacity and impact resistance of sandwich structures can be improved by modifying the thickness ratio of the front-to-back face sheet without modifying the total thickness. However, the published data is inconclusive since better performances with both thinner [4,5] and thicker [6,7] frontal face sheet have been reported.

The main mechanical function of the core in a sandwich panel subjected to impact is to stabilise the face sheets, and to bear shear and out of plain compression loads, and high puncture strength. For this reason, high axial strength unit-cells are of great interest [8,9], and in the field of cellular cores, (also known as architected cellular materials) [10], bio-inspired designs have garnered attention for their outstanding mechanical properties [11]. Among the myriad of designs present in structural applications in nature, the trabecular structure of the forewing of a beetle is the most effective unit-cell reported in the literature [11]. Several authors [12–15] have demonstrated the benefits of this structure in bending and compression, however the impact properties are yet to be reported.

Another promising trend for improving the stiffness, strength, energy absorption, and impact resistance of sandwich structures is substituting conventional uniform honeycomb cores with functionally graded concepts [16]. Several grading features, such as material properties, unit-cell design and size, wall thickness or gradient tendency (weak-to-strong, strong-to-weak, strong-to-weak-to-strong, disordered, etc.) can be modified to tune the properties of the core.

In this context, the present study takes as its focus the out-of-plane behaviour of cores with cell wall thickness variation in the through-thickness direction. This grading approach is almost impossible for conventional manufacturing at present, however additive manufacturing technologies are maturing, and some preliminary studies have been published [17–20] with promising results. Of the functionally graded cores proposed, all presented energy absorption characteristics superior to their uniform counterparts, and the collapse of the structures always started in the thinner layer. Nevertheless, these studies focused solely on the out-of-plane compression of the cellular structures when placed between flat rigid plates behaviour, and no testing was conducted under impact when integrated into a sandwich structure. Consequently,

* Corresponding author.
E-mail address: isukia@mondragon.edu (I. Sukia).

https://doi.org/10.1016/j.compscitech.2024.110515
Received 17 October 2023; Received in revised form 12 February 2024; Accepted 23 February 2024

the effect of positioning the thinner wall under the impacted face sheet or over the rear face sheet remains unknown.

Conventional honeycomb core manufacturing processes are optimised for homogeneous cell structures and flat geometries. However, meeting demanding structural, aerodynamic, and packaging requirements is leading to increasingly complex lightweight parts, and the extra effort required to shape the cores by machining or thermoforming drives up the cost of the final sandwich structures [2]. Additionally, the production of honeycomb sandwich panels requires bonding the face sheets onto the thin cell walls of the core, a critical step in the manufacturing process as it is the weak point of the structure. For curved panels, this bonding poses even greater challenges. Environmental awareness is also growing, and as recycling thermoplastics is easier than thermoset composites and Nomex® cores, interest in fully thermoplastics sandwich panels is on the rise [21]. By way of example, Sam-Daliri et al. [22] used a circular economy approach to show that industrial thermoplastic composite waste could be used as high-quality feedstock for short fibre-reinforced filament in MEX technology.

Hence, new cost-effective and environmentally friendly manufacturing technologies for functionally graded cores of sandwich panels of thermoplastic materials with complex geometries must be explored, and additive manufacturing is emerging as a promising candidate [16]. The principal additive manufacturing technologies for thermoplastic materials are powder bed fusion (Selective Laser Sintering and Multi Jet Fusion) and material extrusion (MEX) [23,24]. Powder bed fusion is well adapted to complex geometries, but the mechanical properties of the materials are limited by the short length of the fibre that can be embedded in the raw material. In the case of MEX, the matrix can be reinforced with long, even continuous fibres, but the design freedom is more limited by the need for support structures and discrete wall-thickness.

Existing published data about additively manufactured cores for sandwich structures can be classified into two categories. The first option is to adhesively bond face sheets to the core [25,26], which presents the same problems as current sandwich structures. The second approach is integral manufacturing using 3D printing, which reduces the cost and improves the adhesion between the core and the face sheets [27–30]. In both categories a fundamental manufacturing consideration is the orientation of the unit cell. In the sandwich with corrugated cores, when the main axis of the cell is parallel to the face sheets, it is printed in a perpendicular build orientation without any support structure [27–29]. In contrast, supports are frequently required when the main axis of the cell is perpendicular to the face sheets, and these are impossible to remove because the sandwich is a closed structure. In a recent study, Sugiyama et al. [30] demonstrated that the fibre-tension generated during the extrusion of filaments with continuous fibre can be high enough to overhang the cellular size, eliminating the need for supports. However, analysis of the literature reveals that the maturity of integrally 3D printed, bio-inspired and functionally graded sandwich structures is low.

Against this backdrop, in the present paper we analyse the impact behaviour of sandwich panels with a core inspired by the trabecular structure of the forewing of a beetle and integrally manufactured with 3D printing. Instrumented falling weight impact tests were used to study the effect of the cell size, the asymmetry of the face sheets thickness, and the wall-thickness variations in the through-thickness direction.

2. Methodology

2.1. Materials and manufacturing

The sandwich panels, integrally 3D printed in a MarkTwo®, were composed of two commercial polyamide composite filaments supplied by Markforged®: (1) a PA6 filled with approximately a 16% by weight of micro carbon fibres named Onyx® for the core, and (2) an amorphous PA 6/3T reinforced with a 36% by weight of continuous carbon fibres (cCFPA) [31] for the face sheets. The main properties of the Onyx® and cCFPA materials were obtained from literature data [31,32] and are summarised in Table 1. The processing parameters for each material were set by the 3D printer supplier. Both filaments are polyamide-based, hence the samples were conditioned in a climatic chamber for four days at 23 °C and 50% relative humidity before testing.

2.2. Specimen description

The sandwich structures were flat, 100 mm circular specimens. The thicknesses of the sandwich (13 mm) and the core (10 mm) were constant for all samples, in accordance with the D 5628-18 standard.

The unit cell design was inspired by the trabecular structure of the forewing of a beetle [12–15]. The diameter of the cylindrical pillars (D) was half of the side length (L) (Fig. 1) and the architecture of the composites in the face sheets of all studied sandwiches was orthotropic. The symmetric face sheet configuration was 8 layers of $[45/\text{-}45]_{2s}$. Each layer thickness was 0.125 mm and was manufactured using a cCFRP in a 3D printer. Each face sheet had 2 Onyx material layers at the bottom and top part of the sheet with the same layer thickness of 0.125 mm.

The first family of configurations focused on the effect of the relative density of the core, obtained by modifying the unit-cell side size between 6 mm and 9 mm, while the thickness of both face sheets was the same (1.5 mm). The samples were named SHD (symmetric high density) and SLD (symmetric low density). According to Y. Li et al. [16], the most significant features of cellular cores are their density and relative density (Table 2), which represents the volume fraction occupied by solid material in the cellular structure. Relative density is the ratio

Table 1
Main mechanical properties of Onyx® and cCFPA.

	Density (kg/m^3)	Elastic Modulus (GPa)	Tensile strength (MPa)	Break strain (%)	
Onyx®	1.18	1.2	53	38	[31]
cCFPA	1.25	69.4	905	1.27	[32]

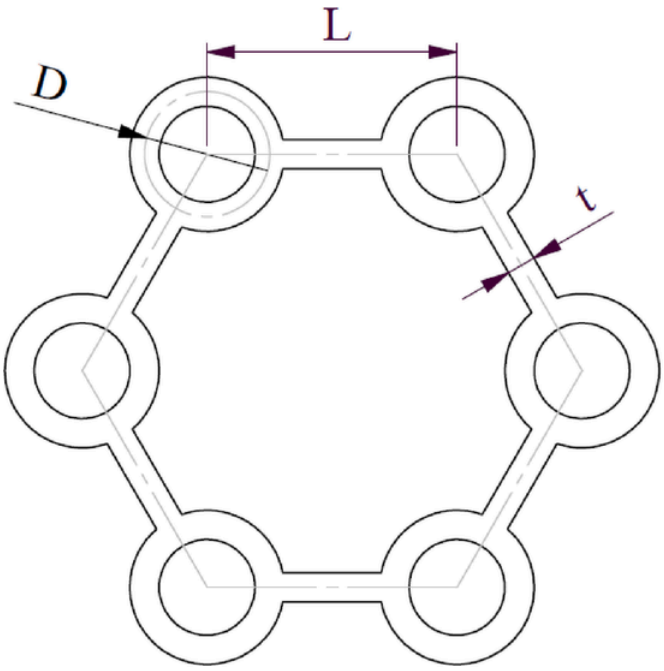

Fig. 1. Trabecular structure design and nomenclature of each variable.

Table 2
Density and relative density values for cores with different cell side sizes.

Sample	L (mm)	Density (kg/m^3)	Relative density
SHD	6	245	0.19
SLD	9	170	0.13

between the density of the architectural element ρ_{eq}, and the density of the bulk material ρ_b, (Onyx® density), and was calculated with Equation (1):

$$\rho_r = \frac{\rho_{eq}}{\rho_b} \tag{1}$$

These relative densities are higher than commercial core grades since the minimum wall thickness (t) obtainable with the MEX 3D printer is thicker. The sandwiches for asymmetry and grading studies were designed with the smallest cell size (6 mm), which facilitated direct comparison of the results of all configurations.

The second family was developed to determine the potential benefits of designing asymmetric face sheets for trabecular-cell cores. The first configuration had an upper (impacted) face sheet thickness of 1 mm, whereas that of the opposite side was 2 mm. The second configuration was geometrically equal, however the impacted face sheet was 2 mm thick.

The third family was used to study the benefits of the trabecular cells with a thickness gradient in the z-direction. Additive manufacturing processes such as SLS [17], DLP [18], and SLA [19] support linear variations of the cell wall in the through-thickness direction. However, in the case of MEX, the wall thickness must be an integer multiple of the deposited bead width. Consequently, the cell walls were composed of three segments of differing thicknesses (0.35 mm, 0.7, and 1.05 mm) and the height of each was equal to the mass of the uniform wall thickness sample. The two grading trends studied were weak-to-strong and strong-to-weak. The face sheet configuration, symmetric or asymmetric, was selected based on the most efficient results. The details of the sandwich configurations are summarised in Table 3.

2.3. Impact test

Low-velocity impact tests were carried out with a drop weight impact machine (Fractovis-Plus Ceast). The impactor was a 20 mm diameter hemispherical head equipped with a 20 kN load-cell, which recorded the force-time data during the impact event. When this force-time curve is integrated based on Newton's second law, displacement-time and energy-time plots can be calculated [33]. Impact samples were clamped with a circular ring of outer and inner diameters of 100 mm and 70 mm, respectively (Fig. 2). The tightening torque for the four clamping screws was 100 Nm. The testing machine was also equipped with an anti-rebound system to prevent multiple collisions that could alter the results. The testing temperature and relative humidity were 23 °C and 55%, respectively.

Characterization consisted of two impact energy levels: 1) 147 J (15 kg released from a height of 1 m, resulting in an initial impact velocity of 4.43 m/s) to induce perforation and characterise the impact behaviour of the sandwich panels, and 2) a supercritical energy level which induced a controlled 10 mm impact displacement to identify the failure mechanism of the core. Perforation energy-displacement curves were used to determine the energy required for 10 mm displacement in each configuration and the mass of the drop weight test was changed to obtain these energy values. New tests were then carried out to induce damage to the specimens in a controlled manner, without affecting the back sheet and limiting the damage to the upper face sheet and the core. A minimum of three samples for each configuration were impact tested to obtain average and standard deviation values.

Table 3
Main features of the sandwich configurations.

Name	Main feature	Face-sheet		Core		Mass (g)	Printing time (min)
		t_{front} (mm)	t_{back} (mm)	L (mm)	t (mm)		
SHD		1.5	1.5	6	0.7	46.2	792
SLD		1.5	1.5	9	0.7	40.5	601
A1/2	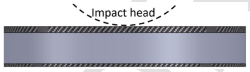	1	2	6	0.7	46.1	810
A2/1	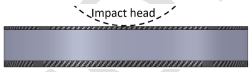	2	1	6	0.7	45.9	810
FG-W/S	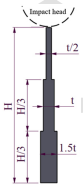	Best results of previous tests		6	0.35–0.7-1.05	47.1	1055
FG-S/W	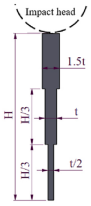			6	1.05–0.7-0.35	47.1	1055

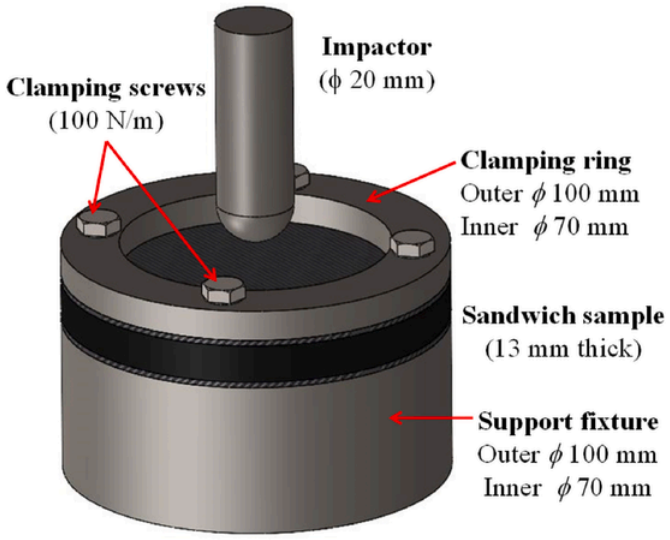

Fig. 2. Impact test set-up.

3. Results and discussion

3.1. Cell-size effect

The typical contact force-displacement impact plots of the sandwich panels presented three distinct stages in the failure process (Fig. 3), which agrees well with other sandwich structures studied in the literature [34,35]. In the first stage, the force increased to a peak (F_{front}), where the front face sheet was damaged and perforated. In the SHD sandwich, the denser core supported the front face sheet, resulting in stiffer sandwich structures. The SHD also provided a stronger substrate to the front face sheet, withstanding a higher peak force (4110 ± 264 N) than the SLD sandwich (2854 ± 330 N).

As regards the deflection at the perforation point, the stiffer SHD structure reported shorter displacements than the SLD sandwich samples. Then, when the front face sheet was perforated, the force dropped suddenly, entering the second stage. In this stage, the trabecular cells of the core still bore compression loads, and the contact force increased up to the core peak (F_{core}). The F_{core} was 4518 ± 145 N in the case of SHD and 4012 ± 103 N for SLD. It should be noted that the compressive strength of the core was higher than that of the frontal face sheet, probably due to the low fibre volume content of the 3D-printed composite. The force after this peak decreased progressively as the cell walls buckled and failed when compressed against the back face sheet. The trans-

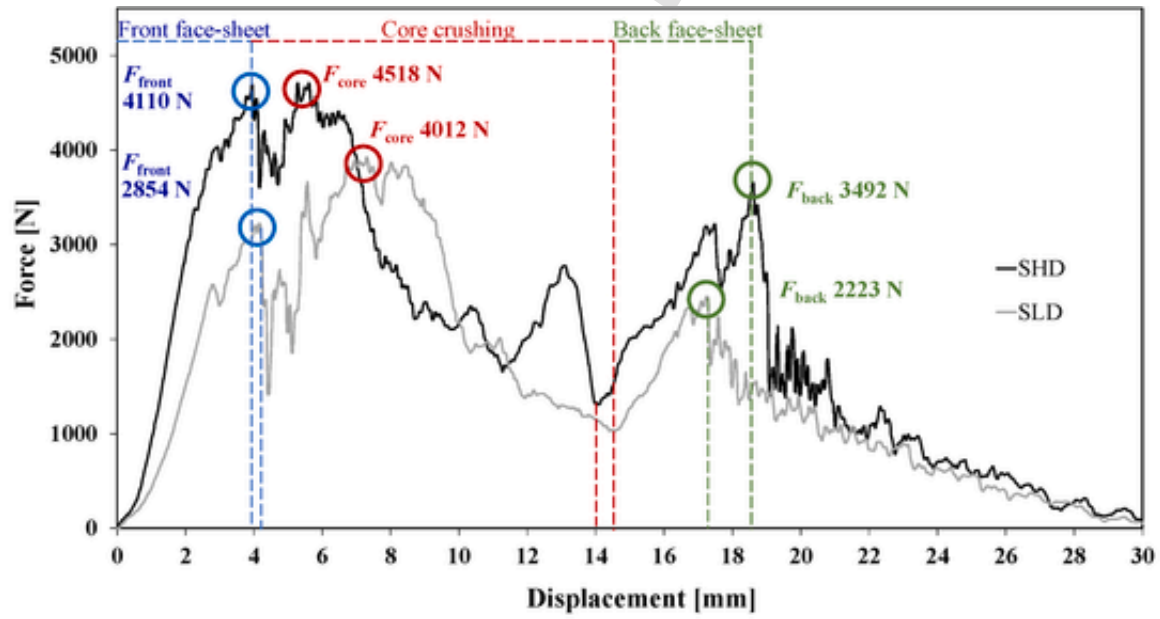

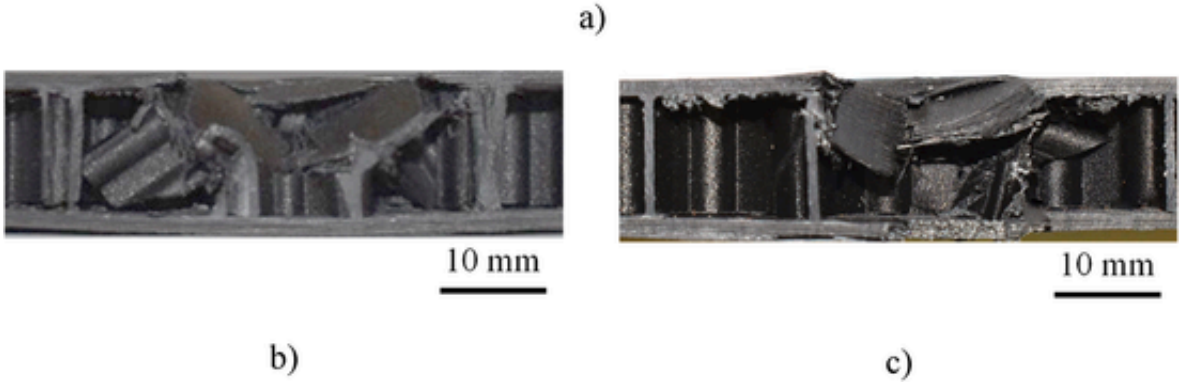

Fig. 3. (a) Contact force-displacement curves for representative SHD and SLD samples impacted with 147 J. Transversal section of the (b) SHD and (c) SLD samples impacted with an incident energy that induced 10 mm of penetration.

versal sections of the SLD (Fig. 3b) and SHD (Fig. 3c) supported the argument that the failure mechanism of the trabecular cell is the same in both samples and that the difference in properties was exclusively due to the denser core of the SHD. It can also be seen that the back face sheet remained undamaged in both samples.

In the third stage, at high crushing strains, the densification of the core transferred the load to the back face sheet, resulting in a final increase in force that peaked at the perforation of the back face sheet (F_{back}). As in the case of the front face sheet, F_{back} was higher for the SHD sandwich (3492 ± 71 N) than the SLD (2223 ± 98 N), which was considerably lower than the corresponding F_{front} values. The displacement at the breaking point of the back face sheet was greater than the nominal thickness of the sandwich panel due to its bending during the impact event. Finally, the cracks generated into the back face sheet propagated, and the impactor perforated it, which resulted in a sudden drop in force. As the impactor maintained sufficient energy, the hemispherical head went through the broken sandwich structure, resulting in a residual frictional force that decreased progressively during the perforation.

Each of these failure processes presented corresponding features in the energy-displacement impact plots (Fig. 4). The absorbed energy up to F_{front} can be considered the amount of energy dissipated by the perforation of the front face sheets (E_{front}). The dissipated energy between the first peak and the inflexion point, where the second peak started, was directly related to the crushing process of the core (E_{core}). This energy dissipated during the rise to the second peak which signalled the perforation of the back face sheet (E_{back}). Finally, the energy plot reached a plateau associated with the total dissipated energy of the sandwich sample (E_{total}). The SHD sandwich curve was always above that of the SLD, indicating that the SHD sandwich performs better for any level of impact energy. Considering the amount of energy dissipated in each failure stage, the SHD values were 48%, 16%, and 145% higher for E_{front}, E_{core}, and E_{back}, respectively. Interestingly, the difference in dissipated energy between the cores was not so pronounced, but a denser core caused higher energy absorption in the face sheet. As a result, the E_{total} of the SHD was 28% higher. The densities of the structures were different, however, and thus the comparison in specific rather than absolute terms are more rigorous. The dissipated specific energy results also favour the SHD structure, as its value of 1.3 J/g was higher than the 1.16 J/g of the SLD sample. This finding is in good agreement with the published results for other 3D printed cell geometries [36].

3.2. Asymmetric face sheet effect

Fig. 5 illustrates the contact force-displacement curves of the asymmetric face sheet sandwich samples impacted with 147 J. As with the symmetric face sheet sandwich samples, the curves can be broken down into three main stages. In the first stage, the initial slope of both sandwiches was the same, indicating that the supporting core compensated for the difference in thickness. However, evidence of damage appeared earlier in sample A1/2, deviating from the linear trend, and progressing with a moderate slope up to the peak where the core started crushing, 4879 ± 161 N. The transition between the front face sheet breaking and the crushing domains of the core was an inflexion point rather than a sharp peak. The initial linear region in the A2/1 sandwich reached 5062 ± 279 N, higher than the 3722 ± 490 N of the A1/2 sandwich, which can be attributed to its thicker front face sheet. Another characteristic feature of the A2/1 was that the strength of the 2 mm thick front face sheet was close to the maximum force of the core, 5406 ± 142 N.

Each cell presented a distinct failure mode, as observed in the transversal section of the samples impacted with an energy level that induced a displacement of 10 mm. In the A1/2 sandwich (Fig. 5b), the cells were compressed because of the high stiffness of the back face sheet. In the A2/1 sandwich (Fig. 5c), the trabecular structure was broken by shearing, as the lower stiffness of the thin back face sheet allowed higher deflections, which in turn reduced the pure compressive stresses. In terms of the structural integrity of the back face sheet, the A2/1 sandwich was almost perforated, and the A1/2 sample remained undamaged. High levels of delamination and fibre breakage were observed in both face sheets.

Thus, generating damage in the A1/2 sandwich sample was easier, as evidenced by its lower F_{front}. In contrast, the damage tolerance of the same sample was higher, as damaging the back face sheet proved more difficult. This behaviour conditioned the last stage, the perforation of the back face sheet. In the A2/1 sample, the thin back face sheet was perforated with a low force, in fact evidence of the perforation was indicated by the sudden force drop rather than by the presence of a force peak. In contrast, the thick back face sheet of the A1/2 sample still bore some load and presented a second peak. Consequently, the force for perforating the thinner back face sheet was 2406 ± 200 N and 4144 ± 26 N for the thicker.

The energy-displacement plot presented the same three stages as the symmetric sandwich (Fig. 6). Both asymmetric sandwich panels absorbed almost the same total energy (≅72 J), which represented 19% more than their symmetric counterpart. This can be attributed to the fact that the core dissipated more energy depending on the sandwich

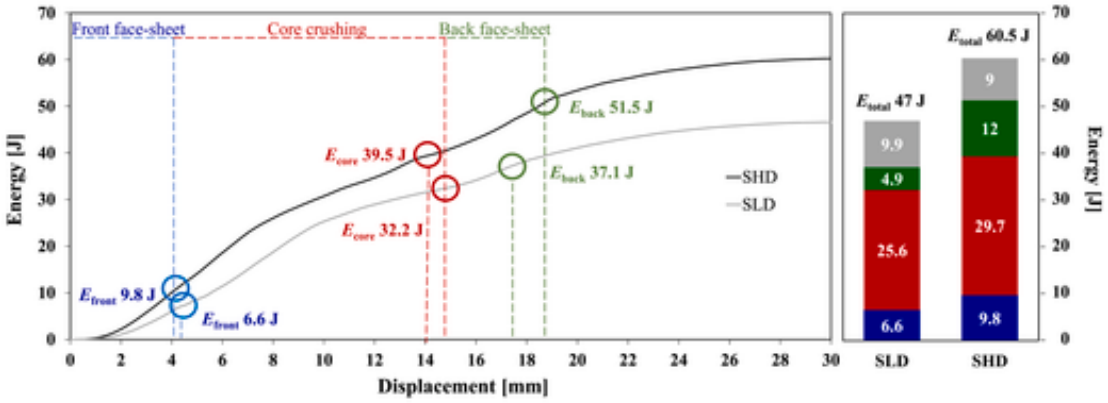

Fig. 4. Absorbed energy-displacement curves for representative SHD and SLD samples impacted with 147 J, and bar chart showing the energy dissipated in each failure stage.

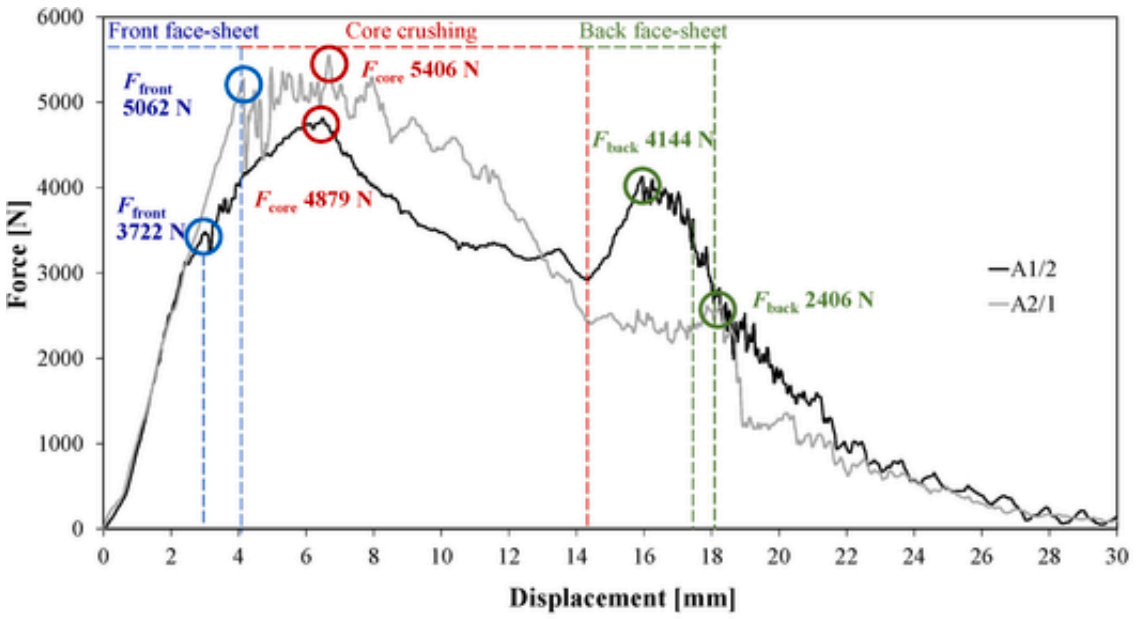

Fig. 5. (a) Representative contact force-displacement curves for A1/2 and A2/1 samples impacted with 147 J. General and zoomed impact-zoom view of the transversal section of the (b) A1/2 and (c) A2/1 samples impacted with incident energy which induced 10 mm of penetration.

face sheet configuration. The face sheets of the A1/2 configuration performed better, as they dissipated 10% more energy than the A2/1. In contrast, the A2/1 core dissipated 13% more impact energy than the A1/2. Once the sample was completely perforated, however, the total dissipated energy was the same for both configurations, since the thinner back face sheet of the A2/1 dissipated less frictional energy. Thus, the selection of the configuration should be driven by the objective: A2/1 performs best in maximising dissipated energy in low incident energy impacts, whereas A1/2 is a better option for damage tolerance. In high-energy impact events, when the sandwich panel is fully perforated, both configurations deliver similar performance.

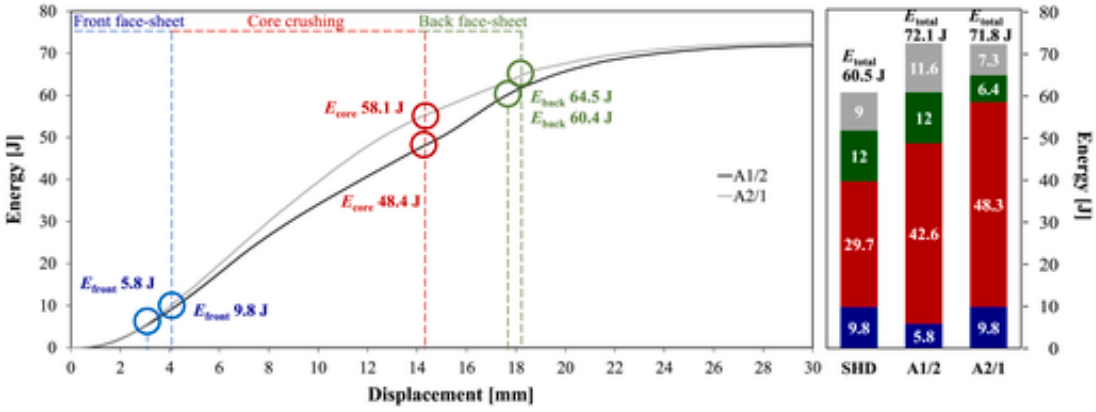

Fig. 6. Representative absorbed energy-displacement curves for A1/2 and A2/1 samples impacted with 147 J, and plot of energy dissipated in each failure stage. SHD results in the bar chart are reference values.

If these results are compared to the published data, it can be seen that the trabecular cell structure more closely resembles the conventional hexagonal honeycomb core [4,5] than the foam cores [6,7]. This is because the thinner top face sheet performs better in honeycomb structures.

3.3. Functionally graded core effect

Based on the results presented in Section 3.2, we selected the A1/2 configuration to further study the functionally graded core because it absorbed the same energy as the A2/1 sandwich but delivered higher tolerance to damage.

The contact force-displacement curves for both thickness grading approaches (Fig. 7) reported different trends, but the failure process followed the same three stages as the previous configurations. In both designs, the load increased up to the perforation of the front face sheets (first peak). However, as the wall thickness of the cells just behind the frontal face sheet in the FG-WS configuration was thinner, the first peak force was 23% lower and took place in smaller displacements. In this same configuration, the load dropped after the first peak due to the collapse of the trabecular core structure, while the strength of the thicker cell walls of the FG-SW caused the load to increase. The most significant differences became apparent during the core crushing: in the FG-WS the load increased progressively due to the growth in thickness, while the FG-SW presented a drop related to the lesser strength of the thinner wall in the deeper layers of the core.

Another key finding was that the maximum load borne by the FG-WS core was 11% higher, which can be explained by the fact that the thick back face sheet allowed the thickest walls to be compressed. However, in the FG-SW configuration, the walls were supported by a weaker thin trabecular structure (Fig. 7 b and c). In the FG-WS core, the cell walls worked like pillars under pure compression, and all segments contributed to the energy dissipation. In contrast, once the front face sheet of the FG-SW configuration was perforated, the cells failed by shearing at the bottom section with the thinner walls, preventing a considerable amount of material from deforming and dissipating any energy.

From a crashworthiness point of view, the fact that the peak load of the FG-WS core was placed further (around 13 mm versus 7.5 mm for the FG-SW) is positive since it indicates lower deceleration. In the last loading stage, both sandwich configurations peaked at the perforation of the back face sheet. Although the thickness was the same, the FG-WS configuration bore a 75% higher load, which demonstrates that locating the thickest walls on the thickest back face sheet produced a synergetic effect.

The influence of these different failure modes on the dissipated energy is plotted in Fig. 8. The figure shows that the FG-WS performed best, as it dissipated 26% more energy than the homogeneous configuration and 42% more than the FG-SW. The superior performance of the FG-SW can be attributed to the front face sheet, since the thickest walls of the core gave it the most robust support. However, the core and back face sheet worked more efficiently in the FG-WS configuration. The FG-SW design also did not favour the proper functioning of the core since it dissipated less energy than all configurations, including the homogeneous wall thickness core solution.

These results demonstrate that the gradient tendency of the core of a sandwich structure has an influence on the energy absorption capacity of the panel. The literature to date has demonstrated the efficiency of such functionally graded cores under out-of-plane compressive loading, where the gradient tendency of the weak-to-strong or strong-to-weak configuration has no influence due to the nature of the test [17–20]. However, in the present study it has been observed that the impact behaviour of the weak-to-strong sandwich core structure is more efficient than the strong-to-weak, due to the synergistic effect of the face sheets and the identified failure modes.

4. Conclusions

This study has analysed the low-velocity impact performance and failure mechanism of integrally 3D-printed sandwich panels using a trabecular structure core based on the forewing of a beetle. A number of design considerations were evaluated, such as the cell size effect, asymmetric face sheets, and functionally graded core designs. The main conclusions are as follows.

1. In all tested cases, the force-displacement curves presented three distinct stages. In the first stage, the perforation of the front face sheet took place up to the first force peak. Core crushing occurred during the second stage, delimited by the lowest force point of the curve. In the third stage, represented by the final force peak, the impactor perforated the back face sheet. Thus, it can be concluded that the proposed sandwich panels behave in the same manner as conventional hexagonal cell honeycomb sandwich panels [8].
2. Honeycomb-like cores 3D printed by extrusion technology were limited in size and the minimum cell dimensions yielded relative densities higher than commercial values [23].
3. The highest density core (3D printed with the smallest cell size) dissipated more energy both in absolute and specific terms, in line with other 3D printed cell structures published in the literature [36].

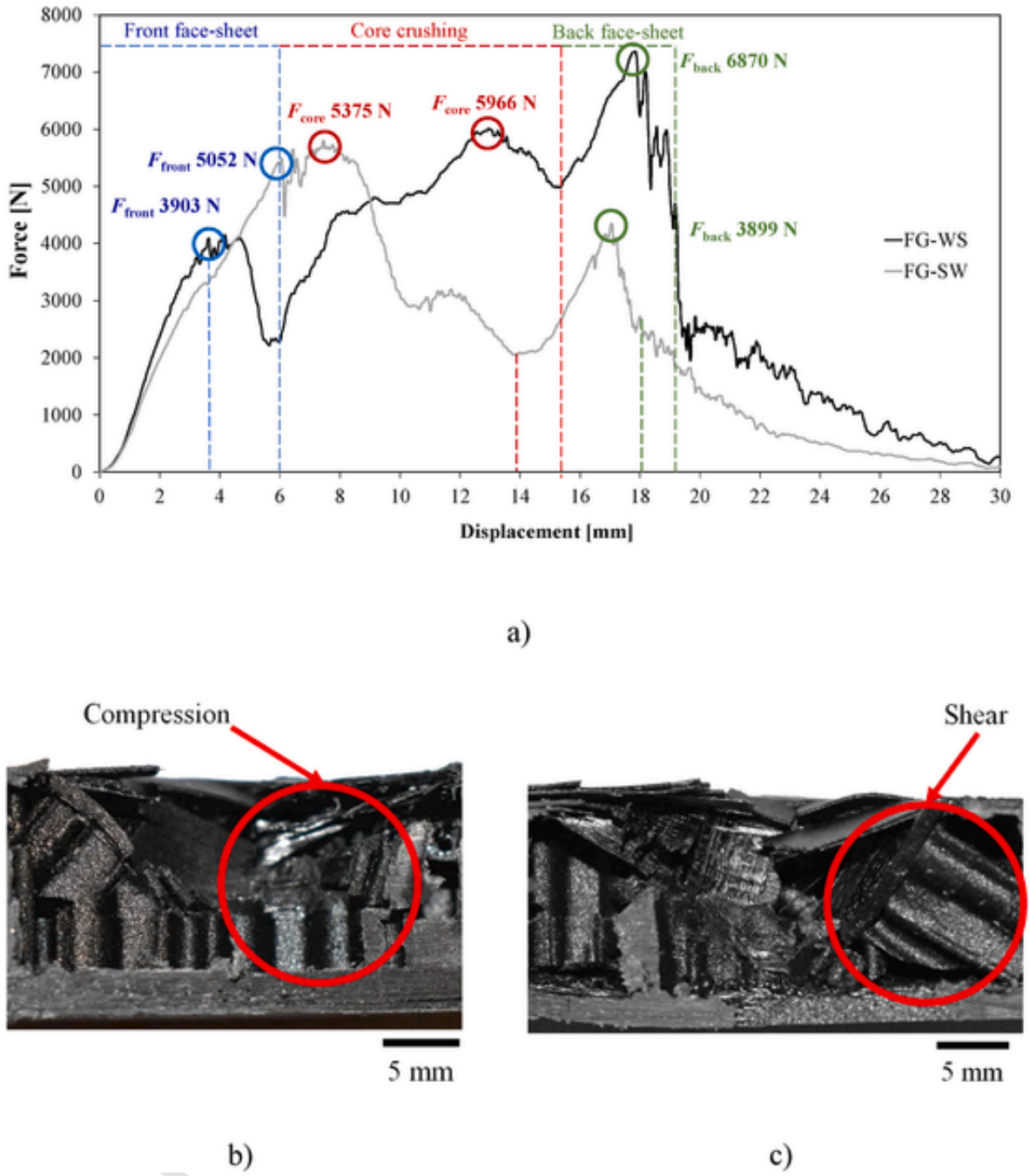

Fig. 7. (a) Representative contact force-displacement curves for FG-WS and FG-SW samples impacted with 147 J. General and zoomed impact-zoom view of the transversal section of the (b) FG-WS and (c) FG-SW samples impacted with incident energy that induced 10 mm of penetration.

4. The asymmetry in both configurations (A1/2 and A2/1) was beneficial in terms of dissipated energy and impact resistance. However, the most effective configuration will depend on the impact energy scenario: the thickest layer should be placed in the front for low-energy impacts, or in the back when damage tolerance is needed. For high-impact energies, the performance of both designs was similar.
5. Varying the thickness of the cell wall of the core in the *z*-direction is feasible due to the design freedom offered by additive manufacturing techniques. However, the efficiency of modifying the thickness from weak-to-strong was higher than grading the wall thickness in the opposite direction. In fact, the weak-to-strong design sandwich plates dissipated the highest impact energy and broke under the highest load. The progressive collapse from the thinner to the thicker cell wall segments gave rise to almost pure compressive behaviour of the cells against the thick back face sheet. On the other hand, when the thicker walls were just behind the front face sheet, the cell walls failed by shearing at the base of the core which prevented the core material contributing to the energy dissipation mechanism.
6. There is general agreement in the literature related to wall thickness gradients that functionally graded structures perform better than homogeneous core structures [17–20]. However, as these studies all tested out-of-plane compression configurations, the effect of gradient tendency was not discussed. A significant finding from the present work is that gradient tendency does have an impact, as the weak-to-strong trend is stronger than the homogeneous wall thickness cell. Nonetheless, the strong-to-weak

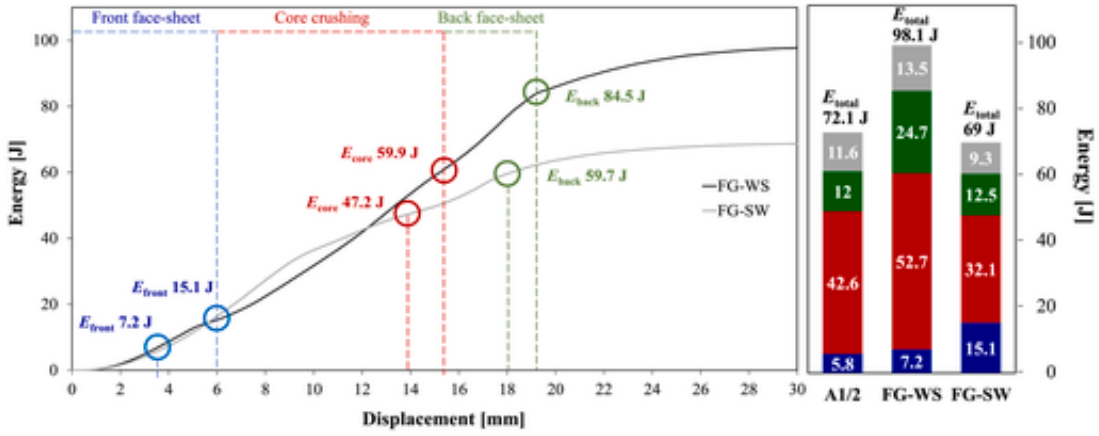

Fig. 8. Absorbed energy-displacement curves for representative FG-WS and FG-SW samples impacted with 147 J and a plot of energy dissipated in each failure stage. A1/2 results in the bar chart are reference values.

gradient performed worse than the homogeneous configuration, which was observed during the impact test result analysis. For out-of-plain tests the functionally graded direction was not found to be significant, whereas it is a critical design parameter in impact energy absorption capacity.

CRediT authorship contribution statement

I. Sukia: Writing – review & editing, Writing – original draft, Software, Investigation. **A. Esnaola:** Writing – review & editing, Validation, Methodology. **B. Erice:** Writing – review & editing, Investigation. **J. Aurrekoetxea:** Writing – review & editing, Supervision, Methodology.

Declaration of competing interest

The authors declare that they have no known competing financial interests or personal relationships that could influence the work reported in this paper.

Data availability

No data was used for the research described in the article.

Acknowledgements

The authors would like to acknowledge the Basque Government for providing funding support (IT833-16; KK-2021/00066) for this research. The author Borja Erice would like to acknowledge the support from the Grant RYC2021-033241-I funded by MCIN/AEI/10.13039/501100011033 and by "European Union NextGenerationEU/PRTR".

References

[1] B. Castanie, C. Bouvet, M. Ginot, Review of composite sandwich structure in aeronautic applications, Composites Part C 1 (2020) 100004, https://doi.org/10.1016/j.jcomc.2020.100004.
[2] V. Birman, G.A. Kardomateas, Review of current trends in research and applications of sandwich structures, Compos. B Eng. 142 (2018) 221–240, https://doi.org/10.1016/j.compositesb.2018.01.027.
[3] C. Qi, F. Jiang, S. Yang, Advanced honeycomb designs for improving mechanical properties: a review, Compos. B Eng. 227 (2021) 109393, https://doi.org/10.1016/j.compositesb.2021.109393.
[4] G. Gao, E. Tang, G. Yang, Y. Han, C. Chen, M. Chang, K. Gou, L. He, Energy absorption performance and optimization of combination modes for carbon fiber reinforced plastics/aluminum honeycomb sandwich panels, Polym. Compos. 43 (2022), https://doi.org/10.1002/pc.26356.
[5] Q. Qin, S. Chen, C. Bai, Y. Wang, W. Zhang, On influence of face sheet distributions on low-velocity impact failure of metal honeycomb core sandwich plates, Thin-Walled Struct. 182 (2023) 437–464, https://doi.org/10.1016/j.tws.2022.110202.
[6] G. Sun, E. Wang, H. Wang, Z. Xiao, Q. Li, Low-velocity impact behaviour of sandwich panels with homogeneous and stepwise graded foam cores, Mater. Des. 160 (2018) 1117–1136, https://doi.org/10.1016/j.matdes.2018.10.047.
[7] W. Zhang, Q. Qin, J. Li, K. Li, L.H. Poh, Y. Li, J. Zhang, S. Xie, H. Chen, J. Zhao, Deformation and failure of hybrid composite sandwich beams with a metal foam core under quasi-static load and low-velocity impact, Compos. Struct. 242 (2020) 112175, https://doi.org/10.1016/J.COMPSTRUCT.2020.112175.
[8] Q. Ma, M.R.M. Rejab, J.P. Siregar, Z. Guan, A review of the recent trends on core structures and impact response of sandwich panels, J. Compos. Mater. 55 (2021) 2513–2555, https://doi.org/10.1177/0021998321990734.
[9] A. Charkaoui, N.M. Hassan, Z. Bahroun, Enhancing mechanical properties of cellular core sandwich panels: a review of topological parameters and design improvements, Mater. Res. Express 10 (10) (2023) 102001, https://doi.org/10.1088/2053-1591/acfb60.
[10] T.A. Schaedler, W.B. Carter, Architected cellular materials, Annu. Rev. Mater. Res. 46 (2016) 187–210, https://doi.org/10.1146/annurev-matsci-070115-031624.
[11] N.S. Ha, G. Lu, A review of recent research on bio-inspired structures and materials for energy absorption applications, Composites, Part B 181 (2020) 107496, https://doi.org/10.1016/j.compositesb.2019.107496.
[12] X. Zhang, J. Xie, J. Chen, Y. Okabe, L. Pan, M. Xu, The beetle elytron plate: a lightweight, high-strength and buffering functional-structural bionic material, Sci. Rep. 7 (2017), https://doi.org/10.1038/s41598-017-03767-w.
[13] J. Chen, X. Zhang, Y. Okabe, K. Saito, Z. Guo, L. Pan, The deformation mode and strengthening mechanism of compression in the beetle elytron plate, Mater. Des. 131 (2017) 948–961, https://doi.org/10.1016/j.matdes.2017.06.014.
[14] J. Chen, X. Yu, M. Xu, Y. Okabe, X. Zhang, W. Tuo, The compressive properties and strengthening mechanism of the middle-trabecular beetle elytron plate, J. Sandw. Struct. Mater. 22 (2020) 948–961, https://doi.org/10.1177/1099636218777188.
[15] X. Zhang, J. Chen, Y. Okabe, P. Zhang, X. Xiong, X. Yu, Influence of honeycomb dimensions and forming methods on the compressive properties of beetle elytron plates, J. Sandw. Struct. Mater. 22 (2020) 28–39, https://doi.org/10.1177/1099636217731993.
[16] Y. Li, Z. Feng, L. Hao, L. Huang, C. Xin, Y. Wang, E. Bilotti, K. Essa, H. Zhang, Z. Li, F. Yan, T. Pejis, A review on functionally graded materials and structures via additive manufacturing: from multi-scale design to versatile functional properties, Advanced Materials Technologies 5 (2020) 1900981, https://doi.org/10.1002/admt.201900981.
[17] I. Maskery, A. Hussey, A. Panesar, A. Aremu, C. Tuck, I. Ashcroft, R. Hague, An investigation into reinforced and functionally graded lattice structures, J. Cell. Plast. 53 (2017) 151–165, https://doi.org/10.1177/0021955X16639035.
[18] J. A.J, J. Schneider, A. Schiffer, F. Hafeez, S. Kumar, Dynamic crushing of tailored honeycombs realized via additive manufacturing, Int. J. Mech. Sci. 219 (2022) 107126, https://doi.org/10.1016/j.ijmecsci.2022.107126.
[19] J.J. Andrew, J. Ubaid, F. Hafeez, A. Schiffer, S. Kumar, Impact performance enhancement of honeycombs through additive manufacturing-enabled geometrical tailoring, Int. J. Impact Eng. 134 (2019) 103360, https://doi.org/10.1016/j.ijimpeng.2019.103360.
[20] Y. Wu, L. Sun, P. Yang, J. Fang, W. Li, Energy absorption of additively manufactured functionally bi-graded thickness honeycombs subjected to axial loads, Thin-Walled Struct. 164 (2021) 107810, https://doi.org/10.1016/j.tws.2021.107810.
[21] J. Grünewald, P. Parlevliet, V. Altstädt, Manufacturing of thermoplastic

composite sandwich structures: a review of literature, J. Thermoplast. Compos. Mater. 30 (2017) 437–464, https://doi.org/10.1177/0892705715604681.
[22] O. Sam-Daliri, P. Ghabezi, J. Steinbach, T. Flanagan, W. Finnegan, S. Mitchell, N. Harrison, Experimental study on mechanical properties of material extrusion additive manufactured parts from recycled glass fibre-reinforced polypropylene composite, Compos. Sci. Technol. 241 (2023) 110125, https://doi.org/10.1016/j.compscitech.2023.110125.
[23] X. Li, J. He, Z. Hu, X. Ye, S. Wang, Y. Zhao, B. Wang, Y. Ou, J. Zhang, High strength carbon-fiber reinforced polyamide 6 composites additively manufactured by screw-based extrusion, Compos. Sci. Technol. 229 (2022) 109707, https://doi.org/10.1016/j.compscitech.2022.109707.
[24] S. Park, K. Fu, Polymer-based filament feedstock for additive manufacturing, Compos. Sci. Technol. 213 (2021) 108876, https://doi.org/10.1016/j.compscitech.2021.108876.
[25] A.K. Haldar, V. Managuli, R. Munshi, R.S. Agarwal, Z.W. Guan, Compressive behaviour of 3D printed sandwich structures based on corrugated core design, Mater. Today Commun. 26 (2021) 101725, https://doi.org/10.1016/j.mtcomm.2020.101725.
[26] A.W. Alshaer, D.J. Harland, An investigation of the strength and stiffness of weight-saving sandwich beams with CFRP face sheets and seven 3D printed cores, Compos. Struct. 257 (2021) 113391, https://doi.org/10.1016/j.compstruct.2020.113391.
[27] Z. Hou, X. Tian, J. Zhang, D. Li, 3D printed continuous fibre reinforced composite corrugated structure, Compos. Struct. 184 (2018) 1005–1010, https://doi.org/10.1016/j.compstruct.2017.10.080.
[28] C. Zeng, L. Liu, W. Bian, J. Leng, Y. Liu, Bending performance and failure behavior of 3D printed continuous fiber reinforced composite corrugated sandwich structures with shape memory capability, Compos. Struct. 262 (2021) 113626, https://doi.org/10.1016/j.compstruct.2021.113626.
[29] H.J. Um, J.S. Lee, J.H. Shin, H.S. Kim, 3D printed continuous carbon fiber reinforced thermoplastic composite sandwich structure with corrugated core for high stiffness/load capability, Compos. Struct. 291 (2022) 115590, https://doi.org/10.1016/j.compstruct.2022.115590.
[30] K. Sugiyama, R. Matsuzaki, M. Ueda, A. Todoroki, Y. Hirano, 3D printing of composite sandwich structures using continuous carbon fiber and fiber tension, Composer Part A Appl. Sci. Manuf. 113 (2018) 114–121, https://doi.org/10.1016/j.compositesa.2018.07.029.
[31] C. Pascual-González, M. Iragi, A. Fernández, J.P. Fernández-Blázquez, L. Aretxabaleta, C.S. Lopes, An approach to analyse the factors behind the micromechanical response of 3D-printed composites, Composites, Part B 186 (2020) 107820, https://doi.org/10.1016/j.compositesb.2020.107820.
[32] M. Iragi, C. Pascual-González, A. Esnaola, C.S. Lopes, L. Aretxabaleta, Ply and interlaminar behaviours of 3D printed continuous carbon fibre-reinforced thermoplastic laminates; effects of processing conditions and microstructure, Addit. Manuf. 30 (Dec. 2019) 100884, https://doi.org/10.1016/J.ADDMA.2019.100884.
[33] S.Z.H. Shah, S. Karuppanan, P.S.M. Megat-Yusoff, Z. Sajid, Impact resistance and damage tolerance of fiber reinforced composites: a review, Compos. Struct. 217 (2019) 100–121, https://doi.org/10.1016/j.compstruct.2019.03.021.
[34] X. Huo, H. Liu, Q. Luo, G. Sun, Q. Li, On low-velocity impact response of foam-core sandwich panels, Int. J. Mech. Sci. 181 (2020), 105681 https://doi.org/10.1016/j.ijmecsci.2020.105681, July.
[35] X. Huo, G. Sun, H. Zhang, X. Lv, Q. Li, Experimental study on low-velocity impact responses and residual properties of composite sandwiches with metallic foam core, Compos. Struct. 223 (April) (2019) 110835, https://doi.org/10.1016/j.compstruct.2019.04.007.
[36] S.A. Saufi, M.Y.M. Zuhri, M.L. Dezaki, S.M. Sapuan, R.A. Ilyas, A. As'arry, M.K.A. Ariffin, M. Bodaghi, Compression behaviour of bio-inspired honeycomb reinforced starfish shape structures using 3d printing technology, Polymers 13 (24) (2021), https://doi.org/10.3390/polym13244388.